Desalination and Water Treatment
www.deswater.com

doi: 10.5004/dwt.2017.20392

67 (2017) 261–270
March

Characterization of magnetic zeolite-polymer composites for Cu(II) and Cr(III) removal from aqueous solutions

Seo-Young Yoon[a], Chang-Gu Lee[b], Jae-Hyun Kim[a], Jin-Kyu Kang[a], Jeong-Ann Park[b], Song-Bae Kim[a,c,*]

[a]*Environmental Functional Materials and Water Treatment Laboratory, Seoul National University, Seoul 08826, Korea, email: songbkim@snu.ac.kr (Song-Bae Kim)*
[b]*Center for Water Resource Cycle Research, Korea Institute of Science and Technology, Seoul 02792, Korea*
[c]*Department of Rural Systems Engineering/Research Institute for Agriculture and Life Sciences, Seoul National University, Seoul 08826, Korea*

Received 9 August 2016; Accepted 26 November 2016

ABSTRACT

The aim of this study was to synthesize and characterize zeolite-based magnetic polymer composites (m-ZPC) for Cu(II) and Cr(III) removal from aqueous solutions. Synthetic zeolite NaA and magnetic iron oxide nanoparticles were immobilized into blended polymer hydrogels composed of poly(vinylidene fluoride) (PVDF) and poly(vinyl alcohol) (PVA) in order to prepare m-ZPC (average particle diameter = 2.97 ± 0.18 mm). Stability tests for m-ZPC against acidic and alkaline solutions indicate that it was stable between solution pHs of 2.0 and 9.0. Batch experiments demonstrate that the maximum adsorption capacities for Cu(II) and Cr(III) were 3.90 and 2.04 mg/g, respectively. The removal of Cu(II) and Cr(III) increased as the pH increased from 2.0 to 5.0. The removal of Cu(II) and Cr(III) was enhanced with a rise of temperature from 15°C to 45°C. In addition, m-ZPC could be reused for Cu(II) removal after regeneration with 5 M NaCl solution. Thermodynamic analyses indicate that the removal of Cu(II) and Cr(III) was endothermic and spontaneous sorption processes (Cu(II): $\Delta H°$ = 115.0 kJ/mol; $\Delta G°$ = –5.13 to –17.64 kJ/mol, and Cr(III): $\Delta H°$ = 73.0 kJ/mol; $\Delta G°$ = –2.50 to –10.36 kJ/mol). This study demonstrates that m-ZPC can be used as a magnetic adsorbent for heavy metal removal in combination with magnetic separation.

Keywords: Chromate; Copper; Magnetic polymer composite; Poly(vinyl alcohol); Poly(vinylidene fluoride)

1. Introduction

Magnetic polymer composites have attracted a considerable amount of recent attention in environmental disciplines because they can be used for contaminant removal and then subsequently separated from water via magnetic attraction [1]. For the preparation of magnetic polymer composites, magnetic iron oxides, such as magnetite (Fe_3O_4) and maghemite (γ-Fe_2O_3), are immobilized into a polymer matrix [2–5]. Additionally, functional materials, including layered double hydroxides [6,7], industrial fungi [8], diethylenetriamine [9], and vermiculite [10], are incorporated for the removal of contaminants. In these composites, the functional materials play a major role in contaminant adsorption, whereas the magnetic iron oxides afford the magnetic properties and play a minor role in contaminant removal [6,10].

Zeolites are microporous and crystalline aluminosilicates that consist of tetrahedral silica (Si) and alumina (Al) units. The isomorphous replacement of Si(IV) by Al(III) contributes to the negatively charged zeolites. Furthermore, these negative charges are balanced by exchangeable cations, such as sodium (Na), potassium (K), and calcium (Ca), which provide

* Corresponding author.

zeolites with cation ion-exchange properties. Therefore, zeolites are widely used as adsorbents for heavy metal cations [11–15]. Recently, some researchers [16–18] have prepared zeolite-based non-magnetic polymer (clinoptilolite–chitosan) composites for the removal of heavy metals such as Cu(II), Co(II), and Ni(II) from aqueous solutions. However, studies related to the zeolite-based magnetic polymer composites (m-ZPC) for heavy metal removal are still scarce. Only one study has been recently reported by Mthombeni et al. [19] who synthesized clinoptilolite–polypyrrole magnetic composites for the adsorption of Cr(VI) from aqueous solutions.

In the present study, synthetic zeolite NaA and magnetic iron oxide nanoparticles were immobilized into blended polymer hydrogels composed of poly(vinylidene fluoride) (PVDF) and poly(vinyl alcohol) (PVA). PVDF is a hydrophobic polymer with excellent chemical resistance, high strength, and physical and thermal stability. Due to its hydrophobicity, however, hydrophilic modification via blending with other polymeric materials is necessary in order to use PVDF in water treatment applications [20]. PVA is a hydrophilic polymer with excellent thermal and chemical stability [21,22]. It is known to be miscible with PVDF [20]. PVA-based polymer hydrogels have been synthesized because of its low cost, non-toxicity, biodegradability, and biocompatibility [23,24].

The aim of this study was to synthesize and characterize m-ZPC for the removal of Cu(II) and Cr(III) from aqueous solutions. Cu(II) is a toxic heavy metal ion, which can be found in industrial wastewaters from a variety of sources including acid mine drainage, metal plating, paint manufacturing, and electronics [25]. Cr(III) is a cation of high toxicity, which is frequently present in tannery wastewaters [26]. Batch experiments were conducted to observe the effects of adsorbent concentration, initial adsorbate concentration, reaction time, temperature, solution pH, and reuse on the removal of Cu(II) and Cr(III). The experimental data were analyzed using equilibrium, thermodynamic, kinetic, and diffusion models.

2. Materials and methods

2.1. Preparation of adsorbents

All chemicals used for the tests were purchased from Sigma-Aldrich (St. Louis, MO, USA). Sodium aluminate ($NaAlO_2$) and sodium metasilicate ($Na_2O{\cdot}SiO_2{\cdot}5H_2O$) were used to synthesize zeolite NaA. This was accomplished by following the procedures (hydrothermal method) outlined by the International Zeolite Association Synthesis Commission. Magnetic iron oxide nanoparticles were synthesized using the co-precipitation method described in our previous researches [27,28]. Briefly, iron sulfate ($FeSO_4{\cdot}7H_2O$) and iron chloride ($FeCl_3{\cdot}6H_2O$) were used for the synthesis of magnetic iron oxide nanoparticles, which are composed of maghemite (γ-Fe_2O_3) and goethite (α-FeOOH) [27]. Based on the synthetic zeolite NaA and magnetic iron oxide nanoparticles, m-ZPC was prepared using two polymers (PVDF and PVA) and polyethylene glycol (pore-forming agent). First, PVDF (11.2 g), PVA (2.8 g), PEG (6 g), zeolite NaA (4.5 g), and magnetic iron oxide nanoparticles (1.5 g) were added into a round-bottom flask filled with 100 mL of a dimethyl sulfoxide (DMSO) solution. After sealing the flask, the solution was stirred in a heating mantle at 85°C for 12 h to obtain a homogeneous suspension. Using a disposable scalp vein set (needle diameter = 0.7 mm) equipped with a syringe pump (78–1100I, Fisher Scientific, Pittsburgh, PA, USA), the suspension was dropped into a stirred reservoir containing deionized water (flow rate = 4 mL/min). The resulting composites (m-ZPC) were allowed to cure in the same deionized water for 24 h under stirring, and then cured for another 24 h without stirring. Prior to use for batch tests, m-ZPC was prepared as hydrated-state by air-drying at room temperature. Additionally, for the preparation of zeolite-based polymer composites (ZPC), zeolite NaA (6 g) was added to 100 mL of a DMSO solution.

2.2. Characterization of adsorbents

The characteristics of the adsorbents were analyzed by various techniques. Mineralogical and crystalline structural characteristics were analyzed using X-ray diffractometry (XRD; D8 Discover, Bruker, Germany) at the conditions of 1.5406 Å Cu Kα radiation and 0.6°/s scanning speed. Field emission scanning electron microscopy (FESEM), energy-dispersive X-ray spectroscopy (EDS), and color mapping were conducted using FESEM (SUPRA 55VP, Carl Zeiss, Oberkochen, Germany). Nitrogen gas (N_2) adsorption–desorption tests were conducted using a surface area analyzer (BELSORP-max, BEL Japan, Inc., Osaka, Japan) to quantify the total pore volume, average pore diameter, and specific surface area. Size distribution was determined using ImageJ 1.43u software (National Institutes of Health, Bethesda, MD, USA).

The stabilities of adsorbents (ZPC and m-ZPC) against acidic and alkaline solutions were examined at pHs of 2, 7, and 9. The solution pH was adjusted using a 0.1 M HCl solution and a 0.1 M NaOH solution, and monitored with a pH probe (9107BN, Thermo Scientific, Waltham, MA, USA). 2 g of the adsorbents were added into 50 mL polypropylene conical tubes containing 30 mL of the pH-adjusted solutions. The tubes were shaken in a shaking incubator at 30°C at 100 rpm for 12 h, and the weights of the adsorbents were quantified after testing. The swelling ratio (S, %) was calculated with the following formula:

$$S = \frac{(W_2 - W_1)}{W_1} \times 100 \quad (1)$$

2.3. Batch experiments

The Cu(II) sorption tests were performed under batch conditions. Desired concentrations of Cu(II) were made from the stock solution (1,000 mg/L), which was prepared with copper chloride dehydrate ($CuCl_2{\cdot}2H_2O$, Sigma-Aldrich). All experiments were performed in triplicate under ambient conditions (temperature = 30°C). The first set of tests was conducted to observe the influence of the adsorbent dose on the removal of Cu(II) by ZPC and m-ZPC (initial Cu(II) concentration = 100 mg/L; pH = 5). The initial Cu(II) concentration of 100 mg/L is equivalent to 1.57 mmol(Cu)/L. The experiments were performed in 50 mL polypropylene conical tubes containing 17–83 g/L of either ZPC or m-ZPC and 30 mL of the

diluted Cu(II) solution. The tubes were shaken at 100 rpm at 30°C using a shaking incubator (Daihan Science, Seoul, Korea). After 12 h of reaction time, the adsorbents were separated from the solution by filtration through a 0.45-μm cellulose filter. The residual Cu(II) concentration was quantified by inductively coupled plasma–atomic emission spectroscopy (ICP-730ES, Varian, Belrose NSW, Australia).

The second set of tests was performed to observe the influence of the solution pH on the removal of Cu(II) by m-ZPC (initial Cu(II) concentration = 100 mg/L; adsorbent dose = 83 g/L; solution pH = 2–5; reaction time = 12 h). The third set of tests was conducted to observe the removal of Cu(II) by m-ZPC at different Cu(II) concentrations (initial Cu(II) concentration = 50–500 mg/L; adsorbent dose = 83 g/L; pH = 5; reaction time = 12 h). The initial Cu(II) concentrations of 50–500 mg/L are equivalent to 0.79–7.87 mmol/L. The fourth set of tests was conducted to observe the effect of the reaction time on the removal of Cu(II) by m-ZPC (initial Cu(II) concentration = 100 mg/L; adsorbent concentration = 83 g/L; pH = 5; reaction time = 12 h). Additional tests were conducted at 15°C and 45°C to examine the influence of temperature on the removal of Cu(II) by m-ZPC. Finally, the fifth set of tests was conducted to observe the influence of adsorbent reuse on the removal of Cu(II) by m-ZPC (initial Cu(II) concentration = 100 mg/L; adsorbent dose = 83 g/L; pH = 5; reaction time = 12 h). After the removal experiments, the adsorbents were immersed in 40 mL of 5 M NaCl solution for 4 h at 30°C and shaken at 100 rpm using a shaking incubator for regeneration.

The Cr(III) removal experiments were conducted following the same procedures that were used for the Cu(II) removal experiments. The desired concentrations of Cr(III) were prepared by diluting the stock solution (1,000 mg/L), which was made with chromium chloride hexahydrate ($CrCl_3 \cdot 6H_2O$, Sigma-Aldrich). In the first set of experiments, the removal of Cr(III) by ZPC and m-ZPC was performed for different adsorbent doses (initial Cr(III) concentration = 100 mg/L; pH = 5; reaction time = 12 h). The initial Cr(III) concentration of 100 mg/L is equivalent to 1.92 mmol(Cr)/L. In the second, third, and fourth sets of experiments, the removal of Cr(III) by m-ZPC was conducted at different solution pHs, Cr(III) concentrations (50–500 mg/L), and reaction times/temperatures, respectively. In the fifth set of experiments, the effect of adsorbent reuse on the removal of Cr(III) by m-ZPC was observed. The Cr(III) concentration was determined by inductively coupled plasma–atomic emission spectroscopy.

2.4. Data analysis

Model parameters were quantified using Microsoft Excel Solver. The following equations of R^2, χ^2, and sum of squared error (SSE) were used for the data analysis:

$$R^2 = \frac{\sum_{i=1}^{m}(y_c - \overline{y_e})_i^2}{\sum_{i=1}^{m}(y_c - \overline{y_e})_i^2 + \sum_{i=1}^{m}(y_c - y_e)_i^2} \quad (2)$$

$$\chi^2 = \sum_{i=1}^{m}\left[\frac{(y_e - y_c)^2}{y_c}\right]_i \quad (3)$$

$$\mathrm{SSE} = \sum_{i=1}^{m}(y_e - y_c)_i^2 \quad (4)$$

3. Results and discussion

3.1. Characteristics of adsorbents

The properties of m-ZPC are presented in Figs. 1–3. The XRD pattern (Fig. 1(a)) shows the peaks of the zeolite synthesized in the laboratory (2θ values: 7.2°, 10.3°, 12.6°, 16.2°, 21.8°, 24.0°, 26.2°, 27.2°, 30.0°, 30.9°, 31.1°, 32.6°, 33.4°, and 34.3°), which agree well with the characteristic peaks of zeolite NaA found in the literature [29]. The FESEM image (inset in Fig. 1(a)) shows that the synthetic zeolite NaA had a hexahedron shape. The characteristics of magnetic iron oxide nanoparticles including particle size, XRD pattern, and FTIR spectra were described in detail elsewhere [27,28]. The saturation magnetization and coercivity of the magnetic iron oxide nanoparticles were 43.29 emu/g and 26.27 Oe, respectively [27]. The digital images (Figs. 1(b) and (c)) demonstrate that ZPC and m-ZPC had light brown and dark brown colors, respectively. Also, m-ZPC was attracted to an external magnet, whereas ZPC was not (insets in Figs. 1(b) and (c), respectively).

The FESEM images of m-ZPC (Figs. 2(a) and (b)) demonstrate that m-ZPC had a sphere shape with various pore sizes inside. The FESEM image (Fig. 2(c)) also shows the zeolite and iron oxide particles embedded in m-ZPC along with the thin polymers. The color mapping (Fig. 2(d)) visualizes the spatial distribution of aluminum (Al, yellow) and silicon (Si, blue), which came from zeolite NaA, and iron (Fe, red), which came from the magnetic iron oxide nanoparticles, on the surfaces of m-ZPC.

The size distribution (Fig. 3(a)) illustrates that m-ZPC had an average particle diameter of 2.97 ± 0.18 mm. The EDS pattern (Fig. 3(b)) demonstrates that the major elements of m-ZPC were carbon (C) and fluorine (F), which came from the blended polymers of PVDF and PVA. Through EDS analysis, C was evident at peak positions of 0.277 and 0.284 keV, which correspond to the K alpha and K beta X-ray signals, respectively. Alternatively, F was evident at peak positions of 0.677 and 0.687 keV, which correspond to the K alpha and K beta X-ray signals, respectively. Also, Fe, Si, Al, and Na were detected at peak positions of 6.403, 1.740, 1.486, and 1.040 keV, respectively, from K alpha X-ray signals. The atomic percentages of m-ZPC were C (52.20%), F (28.51%), O (13.87%), Fe (0.94%), Si (1.83%), Al (1.55%), and Na (1.09%).

According to the Brunauer-Emmett-Teller (BET) analysis, the BET surface area of m-ZPC was 9.58 m^2/g with a total pore volume of 0.0243 cm^3/g and an average pore diameter of 10.13 nm. The Barrett-Joyner-Halenda (BJH) and Horvath-Kawazoe (HK) analyses indicate that the mesopore and micropore volumes of m-ZPC were 0.0243 and 0.0002 cm^3/g, respectively. The swelling ratios of ZPC and m-ZPC are presented in Table 1. The values of *S* were within ±2.4% in all cases, demonstrating that ZPC and m-ZPC (polymer composites made from blended polymers of PVDF and PVA) were stable between solution pHs of 2.0 and 9.0. This indicates that m-ZPC can be applied as an adsorbent in heavy metal removal experiments, which are usually conducted at acidic pH conditions.

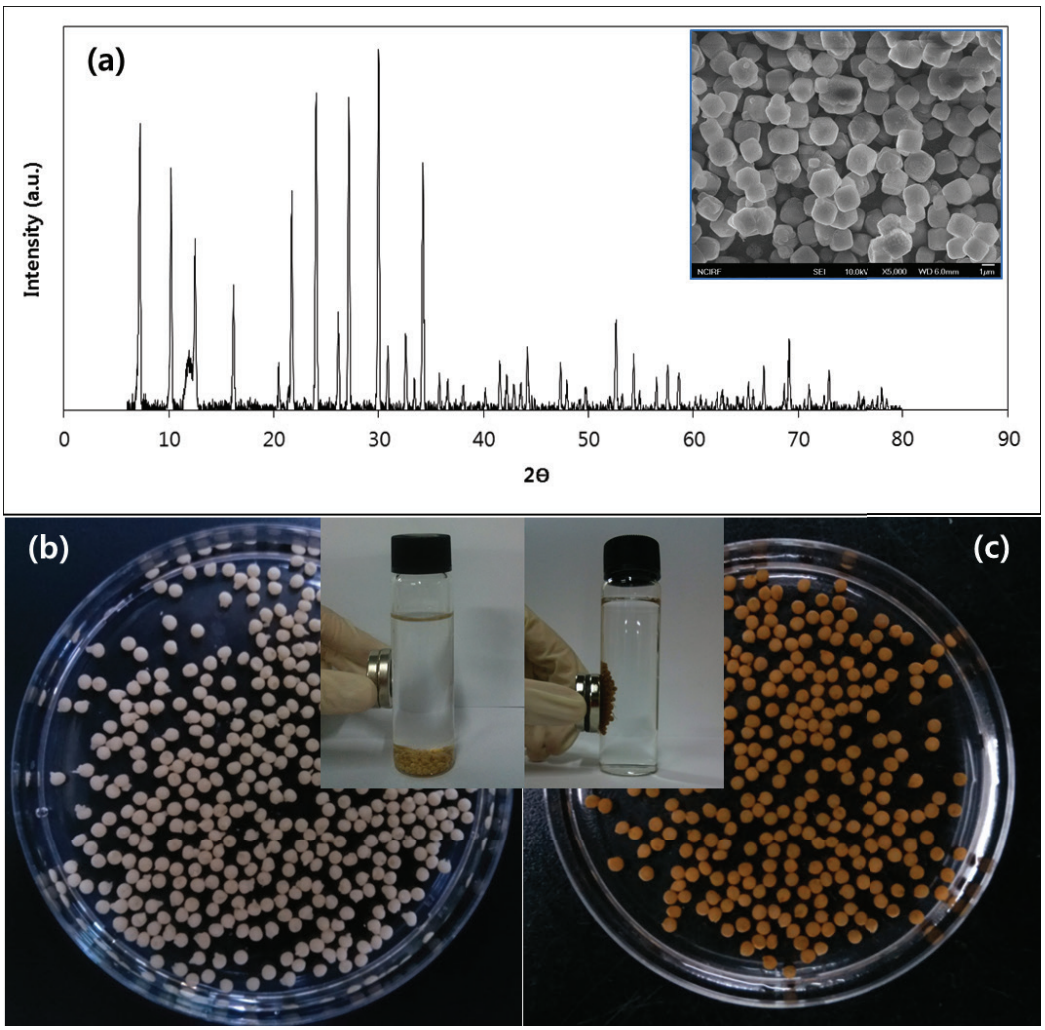

Fig. 1. Characteristics of m-ZPC: (a) XRD pattern of synthetic zeolite (inset = FESEM image; bar = 1 μm), (b) digital image of ZPC (inset = attraction by a magnet in the solution) and (c) digital image of m-ZPC (inset = attraction by a magnet in the solution).

3.2. Characteristics of Cu(II) and Cr(III) removal

The removal of Cu(II) and Cr(III) by ZPC and m-ZPC is compared as a function of the adsorbent dose in Figs. 4(a) and (b), respectively. As the adsorbent dose increased, the adsorption capacities for Cu(II) and Cr(III) decreased gradually, whereas the percentage removal increased gradually. The adsorption capacities of Cu(II) and Cr(III) by m-ZPC were slightly lower than those by ZPC. This could be ascribed to the fact that the quantity of zeolite in m-ZPC was smaller than that in ZPC in grams. However, m-ZPC has an advantage over ZPC due to its magnetic property; m-ZPC can be magnetically separated from aqueous media after treatment of heavy metals in wastewater. Our results demonstrate that the adsorption capacity of Cu(II) by m-ZPC was higher than that of Cr(III) by m-ZPC. This agrees well with findings reported in the literature. Oliveira et al. [30] performed sorption experiments for the removal of Cu(II), Zn(II), and Cr(III) by magnetic NaY zeolites. They reported that the adsorption capacity increased in the order of Cr(III) < Cu(II) < Zn(II). Ismail et al. [31] reported that the adsorption capacity of zeolite A increased in the order of Ni(II) < Cr(III) ≤ Cd(II) < Cu(II). For m-ZPC, the synthetic zeolite NaA played a major role in the removal of Cu(II) and Cr(III). Cu(II) and Cr(III) ions can be removed from aqueous solutions by zeolites via the cation exchange mechanism [31]. During the sorption process, sodium (Na) ions on the surfaces of zeolite NaA are exchanged by Cu(II) and Cr(III) ions in the aqueous phase.

The effect of the solution pH on the removal of Cu(II) and Cr(III) by m-ZPC is presented in Fig. 5(a). The removal of Cu(II) by m-ZPC was affected by the solution pH. The adsorption capacity of Cu(II) at pH 2 (0.42 mg/g) was about three times lower than those at pH 3–5 (1.20–1.21 mg/g). Similar findings have been reported in the literature. Ismail et al. [31] showed that the adsorption percentage of Cu(II) to zeolite A increased from 53% to 100% as the pH increased from 2 to 4. The removal of Cr(III) by m-ZPC was also influenced by the solution pH. The adsorption capacity of Cr(III) at pH 2 (0.41 mg/g) was lower than those at pH 3–5 (1.06–1.18 mg/g). Again, similar results were found in the literature. Wu et al. [32] showed that the adsorption of Cr(III) to zeolites increased as the pH increased from 2.5 and 5.5. Ismail

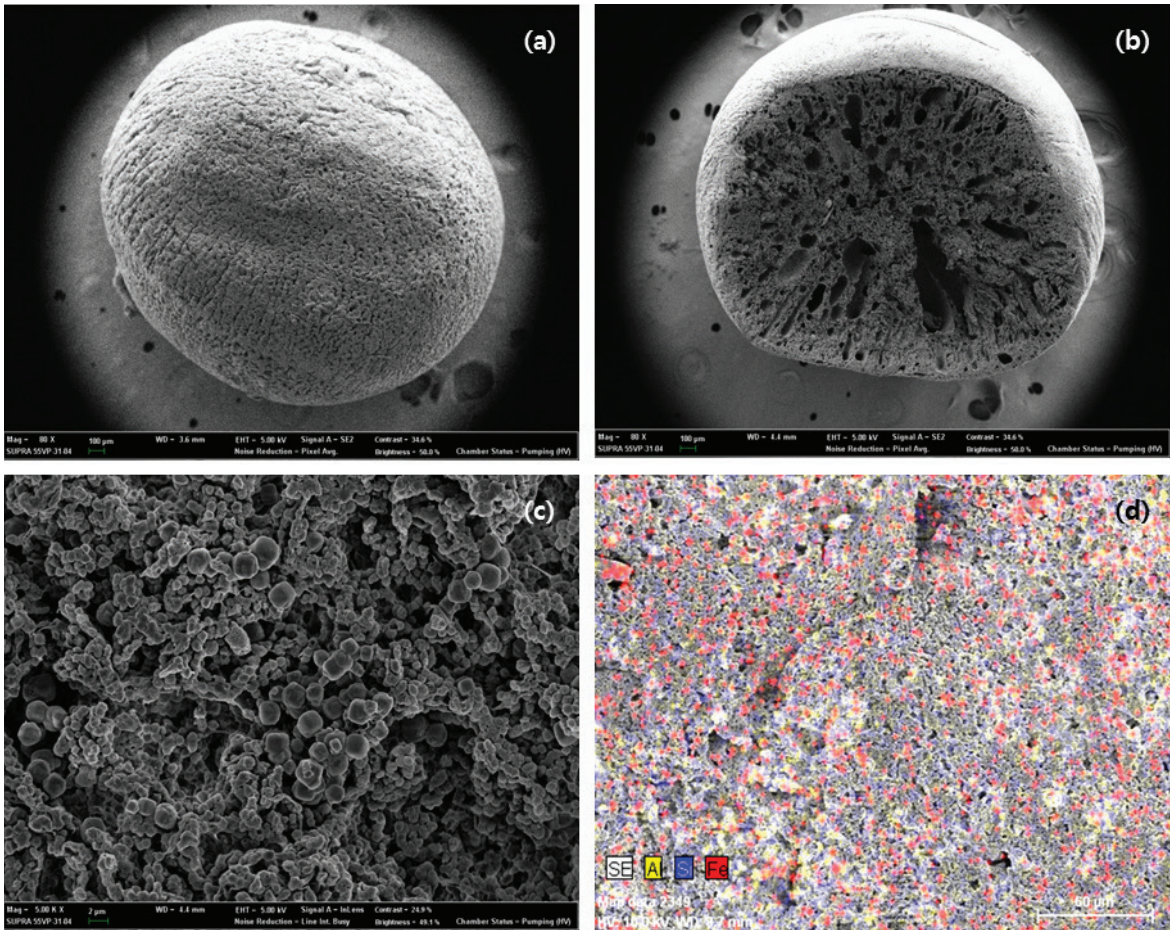

Fig. 2. FESEM images of m-ZPC: (a) overall view of individual composite (bar = 100 μm), (b) cross-sectional view (bar = 100 μm), (c) cross-sectional surface (bar = 2 μm) and (d) color mapping.

et al. [31] found that the adsorption percentage of Cr(III) to zeolite A increased from 50% to 100% as the pH increased from 2 to 4. Note that the speciation of Cr(III) is influenced by the solution pH [32]:

$$Cr^{3+} + H_2O \leftrightarrow Cr(OH)^{2+} + H^+ \quad pK = 4.0 \tag{5}$$

In our experimental conditions (pH 2–5), Cr^{3+} is the predominant form of Cr(III) below pH 4, whereas $Cr(OH)^{2+}$ is the predominant form above pH 4. The poor adsorption of Cu(II) and Cr(III) at highly acidic pH conditions is related to the high competition between hydrogen ions and heavy metal ions for the same sorption sites on the adsorbents.

The removal of Cu(II) and Cr(III) by m-ZPC is presented as a function of the initial adsorbate concentration in Fig. 5(b). In the case of Cu(II), the adsorption capacity increased gradually as the initial Cu(II) concentration increased. The adsorption capacity at a Cu(II) concentration of 50 mg/L was 0.58 mg/g. The adsorption capacity increased to 1.18 mg/g at a Cu(II) concentration of 100 mg/L and further increased to 4.08 mg/g at the highest concentration (500 mg/L). For Cr(III), the adsorption capacity increased from 0.51 to 2.32 mg/g as the Cr(III) concentration increased from 50 to 500 mg/L. These results also show that the adsorption capacity of Cu(II) was greater than that of Cr(III) for all of the initial adsorbate concentrations that were tested.

The removal of Cu(II) and Cr(III) by m-ZPC is presented as a function of the reaction time in Fig. 5(c). In the case of Cu(II), the adsorption capacity increased with increasing reaction time until equilibrium was reached within 12 h. The adsorption capacity of Cu(II) at 30°C rose to 0.90 mg/g after 1 h and further increased to 1.20 mg/g at 12 h. Alternatively, the Cr(III) adsorption capacity at 30°C was 0.63 mg/g at 1 h. This value increased to 1.17 mg/g at 12 h. Similar trends were found for Cu(II) and Cr(III) at 15°C and 45°C.

The effects of adsorbent reuse on Cu(II) and Cr(III) removal by m-ZPC are shown in Fig. 5(d). The Cu(II) removal capacity decreased slightly from 1.19 to 1.01 mg/g during four cycles of reuse. In the case of Cr(III), the removal capacity also decreased from 1.09 to 0.34 mg/g. These results demonstrate that m-ZPC can be reused for Cu(II) removal after regeneration with NaCl solution. Findings in the literature demonstrate that NaCl solution can be successfully used to regenerate zeolites [33,34]. Panayotova [33] reported that natural and modified zeolites, which were used for Cu(II) removal experiments, could be easily regenerated by NaCl solution. Milán et al. [34] also demonstrated that NaCl solution could be used to successfully regenerate exhausted zeolites.

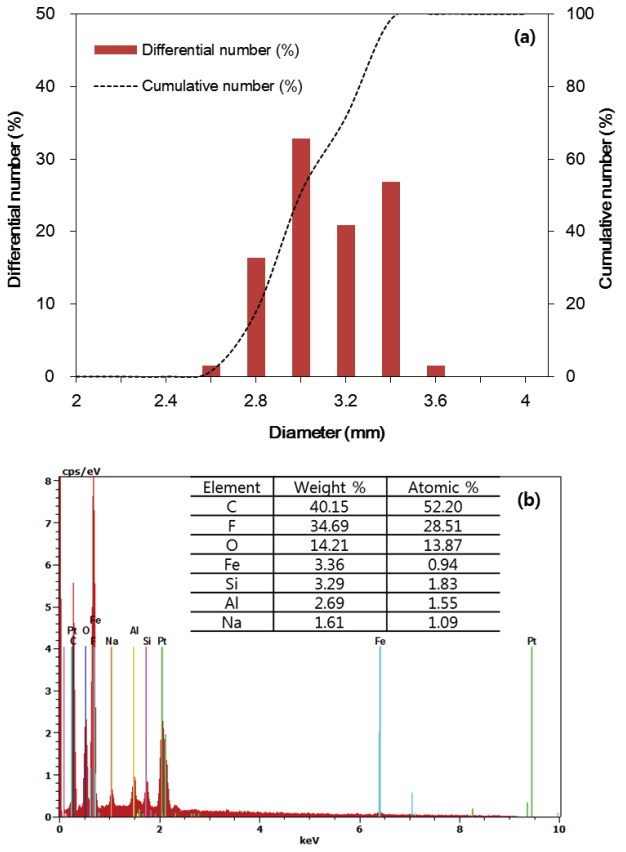

Fig. 3. (a) Size distribution and (b) EDS pattern (inset = element composition) of m-ZPC.

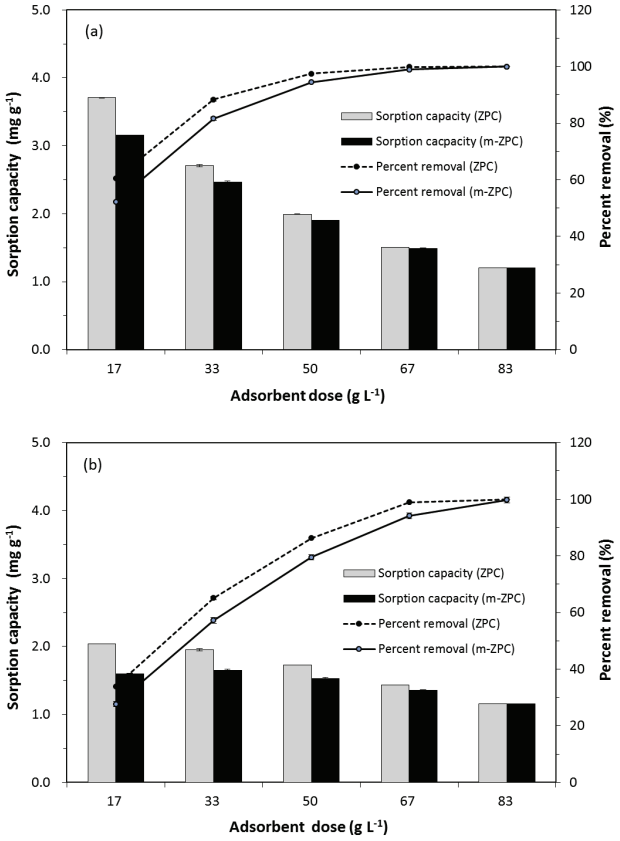

Fig. 4. Sorption capacity of ZPC and m-ZPC under various adsorbent doses: (a) Cu(II) and (b) Cr(III).

Table 1
Swelling ratio (%) of ZPC and m-ZPC at various pH conditions

	pH 2	pH 7	pH 9
ZPC	–1.3	0.1	0.4
m-ZPC	–0.2	2.4	1.6

3.3. Sorption model analyses

The experimental data in Fig. 5(b) were analyzed with the following isotherm models:

Freundlich isotherm:

$$q_e = K_F C_e^{\frac{1}{n}} \tag{6}$$

Langmuir isotherm:

$$q_e = \frac{Q_m K_L C_e}{1 + K_L C_e} \tag{7}$$

Redlich–Peterson isotherm:

$$q_e = \frac{K_R C_e}{1 + a_R C_e^g} \tag{8}$$

The equilibrium model analyses for the Cu(II) and Cr(III) data are illustrated in Fig. 6(a). The values of R^2, χ^2, and SSE indicate (Table 2) that the equilibrium data were most properly described by the Redlich–Peterson isotherm. The Redlich–Peterson isotherm is a hybrid model that combines the Langmuir and Freundlich equations. It can be applied to either homogeneous or heterogeneous systems to explain sorption over a wide range of concentrations [35]. From the Langmuir isotherm, the maximum adsorption capacity for Cu(II) was quantified to be 3.90 mg/g, which is equivalent to 0.061 mmol(Cu)/g. This value is far lower than the Cu(II) adsorption capacity (11.32 mmol(Cu)/g) reported in the literature [18], which have performed the equilibrium sorption experiment using non-magnetic clinoptilolite–chitosan composites. This difference could be ascribed to the fact that the literature value was obtained from the experiments using the high Cu(II) concentrations ranging from 158.9 to 6,354.6 mg/L (2.5–100 mmol/L) and the dried-state composites (dried under vacuum at 40°C), while our value was determined from the experiments using the Cu(II) concentrations ranging from 50 to 500 mg/L and the hydrated-state composites. In the dried-state, the mass of the polymer composites can be reduced considerably, resulting in the increase of the sorption capacity calculated in gram. In addition, the adsorption capacity tends to increase with an increase of initial contaminant concentration [36]. For Cr(III), the maximum adsorption capacity was determined from our batch experiments to be 2.04 mg/g, which is equivalent to 0.039 mmol(Cr)/g (Table 2).

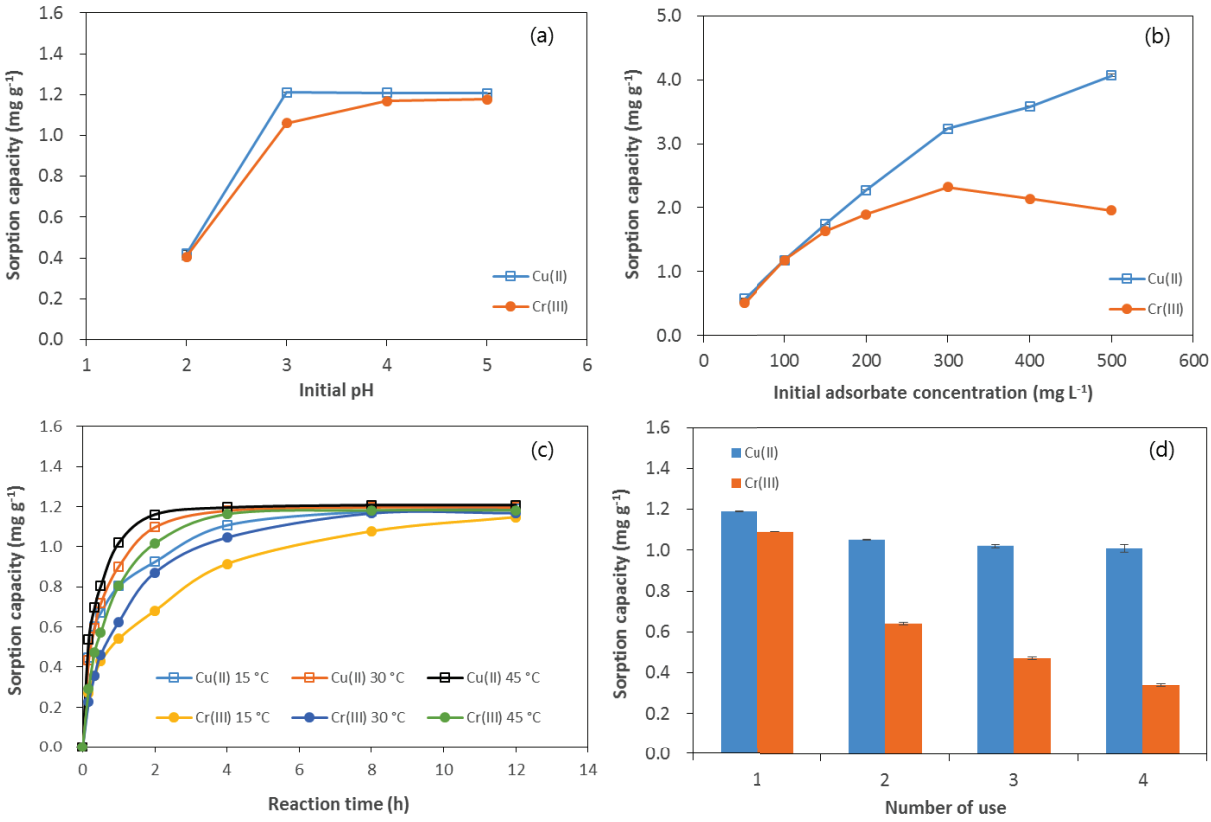

Fig. 5. Sorption of Cu(II) and Cr(III) to m-ZPC at various experimental conditions: (a) solution pH, (b) initial concentration, (c) reaction time and (d) reuse.

The experimental data in Fig. 5(c) were analyzed using the following relationships:

$$\Delta G^{\circ} = \Delta H^{\circ} - T\Delta S^{\circ} \tag{9}$$

$$\Delta G^{o} = -RT\ln K_e; \quad K_e = \frac{aq_e}{C_e} \tag{10}$$

$$\ln\left(K_e\right) = \frac{\Delta S^{\circ}}{R} - \frac{\Delta H^{\circ}}{RT} \tag{11}$$

The thermodynamic analyses for the Cu(II) and Cr(III) data are presented in Fig. 6(b). The thermodynamic parameters are provided in Table 3. The positive values of ΔH° (Cu(II) = 115.0 kJ/mol; Cr(III) = 73.0 kJ/mol) demonstrate the endothermic nature of the sorption processes. The positive values of ΔS° (Cu(II) = 416.9 J/K/mol; Cr(III) = 261.9 J/K/mol) indicate that the randomness increased at the interface between the adsorbent and solution. The negative values of ΔG° (Cu(II) = –5.13 to –17.64 kJ/mol; Cr(III) = –2.50 to –10.36 kJ/mol) show that the sorption of Cu(II) and Cr(III) to m-ZPC were spontaneous. Our results conform well with the study of Panayotova [33], which examined the endothermic and spontaneous adsorption of Cu(II) to natural Bulgarian zeolite. The authors showed that the adsorption percentage of Cu(II) to the zeolite increased as the temperature was increased from 22°C to 50°C. Shawabkeh [37] also demonstrated that the adsorption of Cu(II) on zeolite produced from oil shale ash increased as the temperature was increased from 0°C to 50°C. Mohan et al. [38] reported that the amount of Cr(III) adsorbed on an activated carbon fabric cloth increased as the temperature rose from 10°C to 40°C. However, Zhang et al. [39] reported that the adsorption of Cu(II) on NKF-6 zeolite was spontaneous and exothermic, decreasing with increasing temperature from 20°C to 60°C.

The experimental data in Fig. 5(c) were analyzed using the following kinetic models:

Pseudo-first-order model:

$$q_t = q_e\left(1 - e^{-k_1 t}\right) \tag{12}$$

Pseudo-second-order model:

$$q_t = \frac{k_2 q_e^2 t}{1 + k_2 q_e t} \tag{13}$$

Elovich model:

$$q_t = \frac{1}{\beta}\ln\left(\alpha\beta\right) + \frac{1}{\beta}\ln t \tag{14}$$

The kinetic model analyses for the Cu(II) and Cr(III) data at 15°C are presented as examples in Fig. 6(c). The values of R^2, χ^2, and SSE indicate (Table 4) that the kinetic data

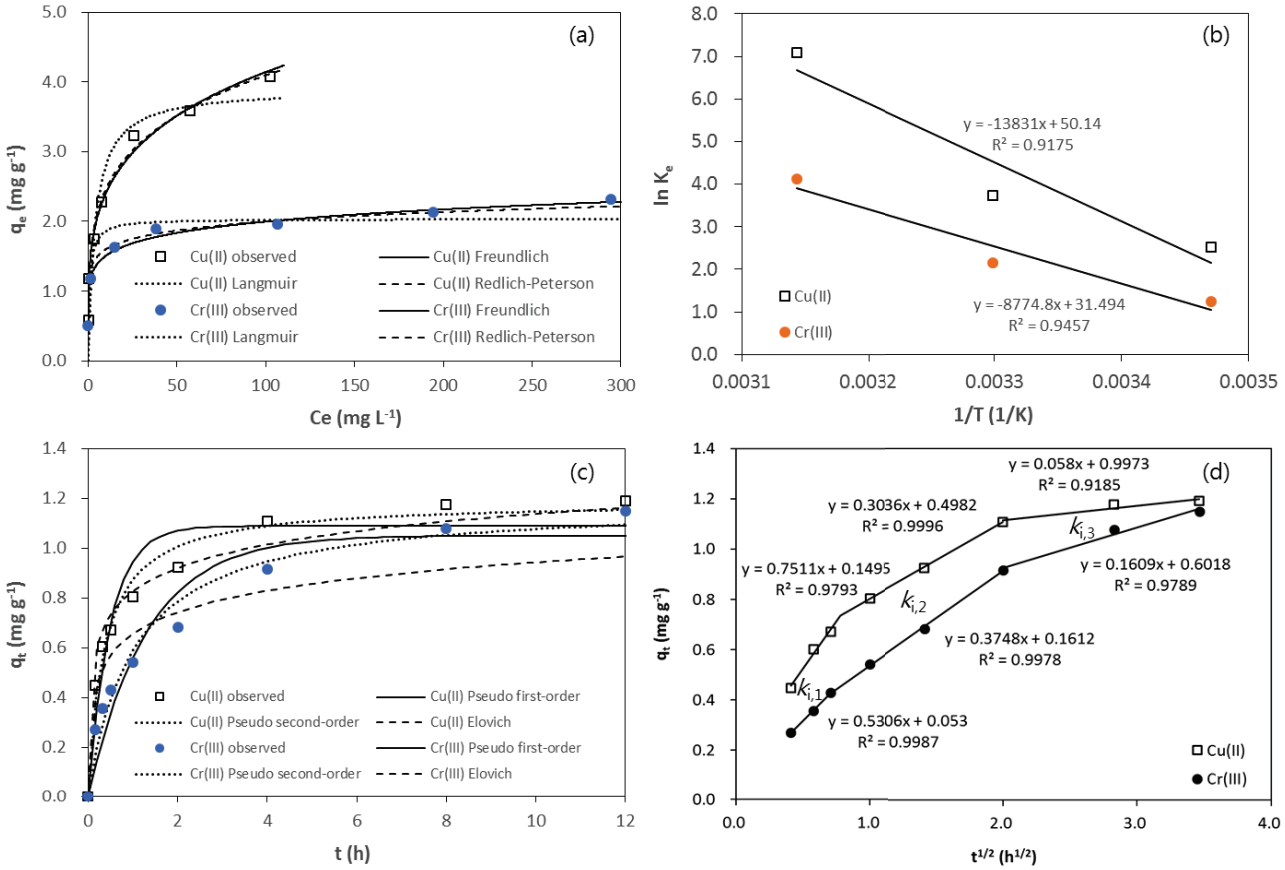

Fig. 6. Model analyses: (a) equilibrium isotherm, (b) thermodynamic model, (c) kinetic sorption model and (d) intraparticle diffusion model. Model parameters are provided in Tables 2–5.

Table 2
Equilibrium isotherm model parameters attained from model fitting to the experimental data

	Freundlich isotherm model					Langmuir isotherm model					Redlich–Peterson model						
	K_F (L/g)	$1/n$	R^2	χ^2	SSE	K_L (L/mg)	Q_m (mg/g)	R^2	χ^2	SSE	K_R (L/g)	a_R (L/mg)	K_R/a_R (mg/g)	g	R^2	χ^2	SSE
Cu(II)	1.39	0.236	0.989	0.074	0.113	0.25	3.90	0.883	5.740	1.190	28.7	19.1	1.50	0.78	0.992	0.038	0.079
Cr(III)	1.14	0.122	0.892	0.159	0.255	1.08	2.04	0.825	5.120	0.413	55.9	43.3	1.29	0.91	0.923	0.091	0.181

Table 3
Thermodynamic parameters attained from model fitting to the experimental data

Temperature (°C)	Cu(II)			Cr(III)		
	$\Delta H°$ (kJ/mol)	$\Delta S°$ (J/K/mol)	$\Delta G°$ (kJ/mol)	$\Delta H°$ (kJ/mol)	$\Delta S°$ (J/K/mol)	$\Delta G°$ (kJ/mol)
15	115.0	416.9	–5.13	73.0	261.9	–2.50
30			–11.38			–6.43
45			–17.64			–10.36

were most properly described by the pseudo-second-order model. From the pseudo-second-order model, the values of q_e and k_2 for Cu(II) were quantified to be 1.19–1.26 mg/g and 2.19–3.28 g/mg/h, respectively. The values of q_e and k_2 for Cr(III) were 1.19–1.28 mg/g and 0.83–1.38 g/mg/h, respectively.

The experimental data in Fig. 5(c) were also analyzed using the intraparticle diffusion model [40]:

$$q_t = k_i t^{1/2} + I \quad (15)$$

Table 4
Kinetic model parameters attained from model fitting to the experimental data

	Temperature (°C)	Pseudo-first-order model					Pseudo-second-order model					Elovich model				
		q_e (mg/g)	k_1 (1/h)	R^2	χ^2	SSE	q_e (mg/g)	k_2 (g/mg/h)	R^2	χ^2	SSE	α (mg/g/h)	β (g/mg)	R^2	χ^2	SSE
Cu(II)	15	1.09	1.97	0.932	0.127	0.083	1.19	2.19	0.982	0.032	0.021	62.1	7.42	0.955	0.060	0.043
	30	1.16	2.02	0.979	0.052	0.029	1.25	2.32	0.997	0.006	0.004	66.5	7.01	0.932	0.111	0.083
	45	1.17	2.68	0.982	0.042	0.024	1.26	3.28	0.995	0.007	0.007	103.7	7.12	0.940	0.075	0.065
Cr(III)	15	1.05	0.76	0.930	0.301	0.083	1.19	0.83	0.971	0.105	0.034	23.9	8.01	0.834	0.241	0.155
	30	1.13	0.90	0.983	0.067	0.025	1.27	0.87	0.997	0.009	0.004	25.1	7.26	0.828	0.318	0.197
	45	1.16	1.34	0.990	0.030	0.014	1.28	1.38	0.997	0.005	0.005	39.6	7.00	0.871	0.238	0.159

Table 5
Diffusion model parameters attained from model fitting to the experimental data (unit = mg g^{-1} $h^{-0.5}$)

Temperature (°C)	Cu(II)			Cr(III)		
	$k_{i,1}$	$k_{i,2}$	$k_{i,3}$	$k_{i,1}$	$k_{i,2}$	$k_{i,3}$
15	0.751	0.304	0.058	0.531	0.375	0.161
30	0.897	0.269	0.012	0.786	0.413	0.086
45	0.951	0.062	0.009	0.951	0.352	0.013

The intraparticle diffusion model analyses for the Cu(II) and Cr(III) data at 15°C are presented as examples in Fig. 6(d). The plots of the intraparticle diffusion model comprised three segments. The first one indicates the diffusion of contaminants through the solution to the external surface of adsorbent (boundary layer diffusion), whereas the second one describes intraparticle diffusion. The third one is attributed to the equilibrium stage where intraparticle diffusion slows down [40,41]. The intraparticle diffusion parameter values ($k_{i,2}$) for Cu(II) were determined to be 0.062–0.304 mg/g/$h^{0.5}$, whereas the values of $k_{i,2}$ for Cr(III) were 0.352–0.413 mg/g/$h^{0.5}$ (Table 5).

4. Conclusions

In this study, m-ZPC was used as an adsorbent for the removal of Cu(II) and Cr(III) ions from aqueous solutions. Batch experiments demonstrate that the adsorption capacity for Cu(II) by m-ZPC was higher than that for Cr(III) by m-ZPC. The removal of Cu(II) and Cr(III) by m-ZPC was enhanced with a rise of temperature from 15°C to 45°C. The adsorption capacity of Cu(II) and Cr(III) by m-ZPC increased with increasing pH between 2.0 and 5.0. In addition, m-ZPC could be reused for Cu(II) removal after regeneration with NaCl solution. Equilibrium model analyses indicate that the Redlich–Peterson isotherm provided the best fit for the equilibrium data. Kinetic model analyses demonstrate that the kinetic data were most properly described by the pseudo-second-order model. Thermodynamic analyses indicate that the removal of Cu(II) and Cr(III) by m-ZPC were endothermic and spontaneous sorption processes. This study demonstrates that m-ZPC can be used as a magnetic adsorbent for heavy metal removal in combination with magnetic separation.

Acknowledgment

This work was supported by the National Research Foundation of Korea, funded by the Ministry of Education, Republic of Korea (grant number 2015–059565).

Symbols

a	—	Adsorbent dose
a_R	—	Redlich–Peterson constant
C_e	—	Equilibrium concentration of Cu(II)/Cr(III) in the aqueous solution
g	—	Redlich–Peterson constant
$\Delta G°$	—	Change in Gibb's free energy
$\Delta H°$	—	Change in enthalpy
I	—	Intercept related to thickness of boundary layer
K_F	—	Freundlich constant related to adsorption capacity
K_L	—	Langmuir constant related to affinity of binding sites
K_R	—	Redlich–Peterson constant
K_e	—	Equilibrium constant (dimensionless)
k_1	—	Pseudo-first-order rate constant
k_2	—	Pseudo-second-order rate constant
k_i	—	Intraparticle diffusion rate constant
$1/n$	—	Freundlich constant related to adsorption intensity
Q_m	—	Maximum adsorption capacity
q_e	—	Amount of Cu(II)/Cr(III) adsorbed at equilibrium
q_t	—	Amount of Cu(II)/Cr(III) adsorbed at time t
R	—	Gas constant
R^2	—	Determination coefficient
SSE	—	Sum of squared error
$\Delta S°$	—	Change in entropy
W_1	—	Weight of the adsorbents before testing
W_2	—	Weight of the adsorbents after testing
y_c	—	Calculated removal capacity from the model
y_e	—	Measured removal capacity from the experiment,
$y_{\bar{e}}$	—	Average of the measured removal capacity
α	—	Initial adsorption rate constant
β	—	Elovich adsorption constant
χ^2	—	Chi-square coefficient

References

[1] S. Kalia, S. Kango, A. Kumar, Y. Haldorai, B. Kumari, R. Kumar, Magnetic polymer nanocomposites for environmental and biomedical applications, Colloid Polym. Sci., 292 (2014) 2025–2052.

[2] A. Idris, N. Hassan, R. Rashid, A.F. Ngomsik, Kinetic and regeneration studies of photocatalytic magnetic separable beads for chromium(VI) reduction under sunlight, J. Hazard. Mater., 186 (2011) 629–635.

[3] X. Wang, C. Zhao, P. Zhao, P. Dou, Y. Ding, P. Xu, Gellan gel beads containing magnetic nanoparticles: an effective biosorbent for the removal of heavy metals from aqueous system, Bioresour. Technol., 100 (2009) 2301–2304.

[4] X. Peng, F. Xu, W. Zhang, J. Wang, C. Zeng, M. Niu, E. Chmielewska, Magnetic Fe_3O_4@silica−xanthan gum composites for aqueous removal and recovery of Pb^{2+}, Colloids Surf., A, 443 (2014) 27–36.

[5] A.E. Chávez-Guajardo, J.C. Medina-Llamas, L. Maqueira, C.A.S. Andrade, K.G.B. Alves, C.P. de Melo, Efficient removal of Cr (VI) and Cu (II) ions from aqueous media by use of polypyrrole/maghemite and polyaniline/maghemite magnetic nanocomposites, Chem. Eng. J., 281 (2015) 826–836.

[6] C.G. Lee, J.A. Park, I. Lee, J.K. Kang, S.Y. Yoon, S.B. Kim, Preparation of magnetic alginate-layered double hydroxide composite adsorbents and removal of Cr(VI) from aqueous solution, Water Sci. Technol. Water Supply, 13 (2013) 846–853.

[7] C.G. Lee, S.B. Kim, Magnetic alginate-layered double hydroxide composites for phosphate removal, Environ. Technol., 34 (2013) 2749–2756.

[8] H. Li, Z. Li, T. Liu, X. Xiao, Z. Peng, L. Deng, A novel technology for biosorption and recovery hexavalent chromium in wastewater by bio-functional magnetic beads, Bioresour. Technol., 99 (2008) 6271–6279.

[9] H. Li, S. Bi, L. Liu, W. Dong, X. Wang, Separation and accumulation of Cu(II), Zn(II) and Cr(VI) from aqueous solution by magnetic chitosan modified with diethylenetriamine, Desalination, 278 (2011) 397–404.

[10] L.C.R. Machado, F.W.J. Lima, R. Paniago, J.D. Ardisson, K. Sapag, R.M. Lago, Polymer coated vermiculite–iron composites: novel floatable magnetic adsorbents for water spilled contaminants, Appl. Clay Sci., 31 (2006) 207–215.

[11] E. Alvarez-Ayuso, A. Garcia-Sanchez, X. Querol, Purification of metal electroplating waste waters using zeolites, Water Res., 37 (2003) 4855–4862.

[12] B. Biškup, B. Subotic, Kinetic analysis of the exchange processes between sodium ions from zeolite A and cadmium, copper and nickel ions from solutions, Sep. Purif. Technol., 37 (2004) 17–31.

[13] D. Nibou, H. Mekatel, S. Amokrane, M. Barkat, M. Trari, Adsorption of Zn^{2+} ions onto NaA and NaX zeolites: kinetic, equilibrium and thermodynamic studies, J. Hazard. Mater., 173 (2010) 637–646.

[14] V. Hernandez-Montoya, M.A. Perez-Cruz, D.I. Mendoza-Castillo, M.R. Moreno-Viergen, Competitive adsorption of dyes and heavy metals on zeolitic structures, J. Environ. Manage., 16 (2013) 213–221.

[15] G. Asgari, B. Ramavandi, L. Rasuli, M. Ahmadi, Cr (VI) adsorption from aqueous solution using a surfactant-modified Iranian zeolite: characterization, optimization, and kinetic approach, Desal. Wat. Treat., 51 (2013) 6009–6020.

[16] E.S. Dragan, M.V. Dinu, Removal of copper ions from aqueous solution by adsorption on ionic hybrids based on chitosan and clinoptilolite, Ion Exch. Lett., 2 (2009) 15–18.

[17] E.S. Dragan, M.V. Dinu, D. Timpu, Preparation and characterization of novel composites based on chitosan and clinoptilolite with enhanced adsorption properties for Cu^{2+}, Bioresour. Technol., 101 (2010) 812–817.

[18] M.V. Dinu, E.S. Dragan, Evaluation of Cu^{2+}, Co^{2+} and Ni^{2+} ions removal from aqueous solution using a novel chitosan/clinoptilolite composite: kinetics and isotherms, Chem. Eng. J., 160 (2010) 157–163.

[19] N.H. Mthombeni, M.S. Onyango, O. Aoyi, Adsorption of hexavalent chromium onto magnetic natural zeolite-polymer composite, J. Taiwan Inst. Chem. Eng., 50 (2015) 242–251.

[20] N. Li, C. Xiao, S. An, X. Hu, Preparation and properties of PVDF/PVA hollow fiber membranes, Desalination, 250 (2010) 530–537.

[21] C.C. Huang, C.K. Lin, C.T. Lu, C.W. Lou, C.Y. Chao, J.H. Lin, Evaluation of the electrospinning manufacturing process based on the preparation of PVA composite fibres, Fibres Text. East. Eur., 17 (2009) 34–37.

[22] N.P. Gule, M. de Kwaadsteniet, T.E. Cloete, B. Klumperman, Electrospun poly(vinyl alcohol) nanofibres with biocidal additives for application in filter media, 1–properties affecting fibre morphology and characterisation, Macromol. Mater. Eng., 297 (2012) 609–617.

[23] I. Lee, C.G. Lee, J.A. Park, J.K. Kang, S.Y. Yoon, S.B. Kim, Removal of Cr(VI) from aqueous solution using alginate/polyvinyl alcohol-hematite composite, Desal. Wat. Treat., 51 (2013) 3438–3444.

[24] Y.U. Han, C.G. Lee, J.A. Park, J.K. Kang, I. Lee, S.B. Kim, Immobilization of layered double hydroxide into polyvinyl alcohol/alginate hydrogel beads for phosphate removal, Environ. Eng. Res., 17 (2012) 129–134.

[25] S. Veli, B. Pekey, Removal of copper from aqueous solutions by ion exchange resins, Fresen. Environ. Bull., 13 (2004) 244–250.

[26] C. Covarrubias, R. García, R. Arriagada, J. Yánez, M.T. Garland, Cr(III) exchange on zeolites obtained from kaolin and natural mordenite, Microporous Mesoporous Mater., 88 (2006) 220–231.

[27] S.Y. Yoon, C.G. Lee, J.A. Park, J.H. Kim, S.B. Kim, S.H. Lee, J.W. Choi, Kinetic, equilibrium and thermodynamic studies for phosphate adsorption to magnetic iron oxide nanoparticles, Chem. Eng. J., 236 (2014) 341–347.

[28] J.A. Park, S.B. Kim, C.G. Lee, S.H. Lee, J.W. Choi, Adsorption of bacteriophage MS2 to magnetic iron oxide nanoparticles in aqueous solutions, J. Environ. Sci. Health., Part A., 49 (2014) 1116–1124.

[29] M.J. Treacy, J.B. Higgins, Collection of Simulated XRD Powder Patterns for Zeolites, Elsevier, Amsterdam, The Netherlands, 2001.

[30] L.C.A. Oliveira, D.I. Petkowicz, A. Smaniotto, S.B.C. Pergher, Magnetic zeolites: a new adsorbent for removal of metallic contaminants from water, Water Res., 38 (2004) 3699–3704.

[31] A.A. Ismail, R.M. Mohamed, I.A. Ibrahim, G. Kini, B. Koopman, Synthesis, optimization and characterization of zeolite A and its ion-exchange properties, Colloids Surf., A, 366 (2010) 80–87.

[32] D. Wu, Y. Sui, S. He, X. Wang, C. Li, H. Kong, Removal of trivalent chromium from aqueous solution by zeolite synthesized from coal fly ash, J. Hazard. Mater., 155 (2008) 415–423.

[33] M. Panayotova, Kinetics and thermodynamics of copper ions removal from wastewater by use of zeolite, Waste Manage., 21 (2001) 671–676.

[34] Z. Milán, S. Montalvo, C.D.L. Pozas, O. Monroy, E. Sánchez, R. Borja, The effects of hydraulic loading and NaCl concentrations on the regeneration of exhausted homoionic natural zeolite, J. Environ. Sci. Health., Part A, 46 (2011) 596–600.

[35] K.Y. Foo, B.H. Hameed, Insights into the modeling of adsorption isotherm systems, Chem. Eng. J., 156 (2010) 2–10.

[36] R. Ocampo-Perez, R. Leyva-Ramos, J. Mendoza-Barron, R.M. Guerrero-Coronado, Adsorption rate of phenol from aqueous solution onto organobentonite: surface diffusion and kinetic models, J. Colloid Interface Sci., 364 (2011) 195–204.

[37] R. Shawabkeh, Equilibrium study and kinetics of Cu^{2+} removal from water by zeolite prepared from oil shale ash, Process Saf. Environ. Prot., 87 (2009) 262–266.

[38] D. Mohan, K.P. Singh, V.K. Singh, Trivalent chromium removal from wastewater using low cost activated carbon derived from agricultural waste material and activated carbon fabric cloth, J. Hazard. Mater., 135 (2006) 280–295.

[39] H. Zhang, D. Zhao, L. Chen, X.J. Yu, Investigation of Cu(II) adsorption from aqueous solutions by NKF-6 zeolite, Water Sci. Technol., 63 (2011) 395–402.

[40] S.K. Bajpai, M.K. Armo, Equilibrium sorption of hexavalent chromium from aqueous solution using iron(III)-loaded chitosan-magnetite nanocomposites as novel sorbent, J. Macromol. Sci., Pure Appl. Chem., 46 (2009) 510–520.

[41] W.H. Cheung, Y.S. Szeto, G. McKay, Intraparticle diffusion process during acid dye adsorption onto chitosan, Bioresour. Technol., 98 (2007) 2897–2904.